Isobaric annealing of high-density amorphous ice between 0.3 and 1.9 GPa: *in situ* density values and structural changes

Christoph G. Salzmann,†*[a] Thomas Loerting,[ab] Stefan Klotz,[c] Peter W. Mirwald,[d] Andreas Hallbrucker[a] and Erwin Mayer[a]

We report *in situ* density values of amorphous ice obtained between 0.3 and 1.9 GPa and 144 to 183 K. Starting from high-density amorphous ice made by pressure-amorphizing hexagonal ice at 77 K, samples were heated at a constant pressure until crystallization to high-pressure ices occurred. Densities of amorphous ice were calculated from those of high-pressure ice mixtures and the volume change on crystallization. In the density *versus* pressure plot a pronounced change of slope occurs at ~ 0.8 GPa, with a slope of 0.21 g cm^{-3} GPa^{-1} below 0.8 GPa and a slope of 0.10 g cm^{-3} GPa^{-1} above 0.8 GPa. Both X-ray diffractograms and Raman spectra of recovered samples show that major structural changes occur up to ~ 0.8 GPa, developing towards those of very high-density amorphous ice reported by (T. Loerting, C. Salzmann, I. Kohl, E. Mayer and A. Hallbrucker, *Phys. Chem. Chem. Phys.*, 2001, **3**, 5355) and that further increase of pressure has only a minor effect. In addition, the effect of annealing temperature (T_A) at a given pressure on the structural changes was studied by Raman spectra of recovered samples in the coupled O–H and decoupled O–D stretching band region: at 0.5 GPa structural changes are observed between ~ 100–116 K, at 1.17 GPa between ~ 121–130 K. Further increase of T_A or of annealing time has no effect, thus indicating that the samples are fully relaxed. We conclude that mainly irreversible structural changes between 0.3 to ~ 0.8 GPa lead to the pronounced increase in density, whereas above ~ 0.8 GPa the density increase is dominated to a large extent by reversible elastic compression. These results seem consistent with simulation studies by (R. Martoňàk, D. Donadio and M. Parrinello, *J. Chem. Phys.*, 2005, **122**, 134501) where substantial reconstruction of the topology of the hydrogen bonded network and changes in the ring statistics from *e.g.* mainly six-membered to mainly nine-membered rings were observed on pressure increase up to 0.9 GPa and further pressure increase had little effect.

Introduction

High-density amorphous ice (HDA) and the apparently first-order transition between HDA and low-density amorphous ice[1,2] (LDA) play a key role in the concept of polyamorphism of one-component systems and the liquid–liquid phase transition hypothesis where a second critical point at low temperature is assumed to cause the anomalous properties of supercooled water[3–6] (for recent reviews see refs. 7–10). In that scenario LDA is the glass associated with a low-density liquid (LDL), whereas HDA is the glass associated with a high-density liquid (HDL). HDA was first made by Mishima *et al.*[1,2] by compression of hexagonal ice (ice Ih) at 77 K and

1.0 GPa (reviewed by Whalley in ref. 11) and the LDA ⇔ HDA transition has been characterized among others by diffraction,[1,2,12–21] change of volume,[2,22–24] heat effects,[22,23,25] Raman spectroscopy,[26–30] ultrasonics and thermal conductivity,[31–34] visually,[30,35] and by simulations (refs. 21, 36–39, with references for older literature). HDA has been considered to be a glassy state of high-pressure liquid water[1,2,23,24,40,41] or a collapsed "ill-crystalline" phase,[42,43] and discussions about these interpretations continue (reviewed in refs. 7,8). Its structure has been argued to be similar to that of high-pressure liquid water which suggests that it is a glassy form of the latter,[8] but its glass transition has not been observed so far.

Loerting *et al.*[44] recently reported that an even denser form of amorphous ice, called very high-density amorphous (VHDA) ice, can be recovered at 77 K and 1 bar, after isobaric heating of HDA at 0.84, 1.1 and 1.9 GPa up to ~ 154 K (at 0.84 GPa), ~ 165 K (at 1.1 GPa) and ~ 177 K (at 1.9 GPa) (reviewed by Klug in ref. 45). VHDA was found to relax on recovering at 77 K and 1 bar to a density of 1.25 ± 0.01 g cm^{-3}, independent of the pressure and temperature it has been taken to. Its density is thus $\sim 9\%$ higher than that of recovered HDA (determined as 1.15 ± 0.01 g cm^{-3} by buoyancy in the same manner as that of VHDA; higher by $\sim 7\%$ if Mishima

[a] *Institute of General, Inorganic and Theoretical Chemistry, University of Innsbruck, A-6020 Innsbruck, Austria. E-mail: christoph.salzmann@gmx.at*
[b] *Institute of Physical Chemistry, University of Innsbruck, A-6020 Innsbruck, Austria*
[c] *Physique des Milieux Denses, IMPMC, CNRS UMR 7590, Université P&M Curie, 4 Place Jussieu, 75252 Paris, France*
[d] *Institute of Mineralogy and Petrography, University of Innsbruck, A-6020 Innsbruck, Austria*
† Present address: Inorganic Chemistry Laboratory, University of Oxford, South Parks Road, Oxford, UK OX1 3QR.

et al.'s[1] density value of 1.17 ± 0.02 g cm^{-3} for HDA is used). The detailed structure of VHDA has been determined by Finney et al.[46] via neutron diffraction with isotope substitution and the number of nearest neighbours was found to increase from 5 in HDA[16] to 6 in VHDA. Debenedetti[9] recently concluded that one of the key unanswered questions in amorphous water research is the relationship between VHDA and HDA, that is "whether it is a distinct phase, separated from HDA by a first-order transition, or whether it is simply very dense HDA". Klotz et al.[47–49] pointed out that the local structure of recovered VHDA is very similar to that of HDA at ~ 0.7 GPa and 100 K. Ref. 37–39, 49–52 list recent simulation studies of VHDA and ref. 18,33,48,53,54 list experimental studies. The consensus of the simulation studies on VHDA seems to be that it is a relaxed form of HDA obtained on heating and annealing of HDA under pressure and that VHDA should be considered as the amorphous ice associated with HDL rather than HDA. However, HDA and VHDA were also attributed to distinct phases, called phase III and phase IV, in computer simulation studies of various water models with three liquid–liquid phase transitions.[55,56]

Here we report in situ density values of high-density amorphous ice obtained between 0.3 and 1.9 GPa and 144 to 183 K. The measurement of densities of amorphous samples under in situ pressure conditions is experimentally difficult and not possible by e.g. diffraction experiments. However, the densities of the various crystalline high-pressure ice phases are known as a function of pressure and temperature. In this paper we make use of this fact and calculate the densities of amorphous ice under pressure from those of the crystalline high-pressure ices formed on isobaric heating of HDA and the volume change (ΔV_c) on crystallization. These volume changes are determined by extrapolation within a narrow temperature region which circumvents the obstacle of unknown apparatus functions in the piston cylinder experiments. Most of the isobaric crystallization experiments used for this study are described in detail in our recent study on the isobaric crystallization properties of HDA under pressure.[57]

We further relate the in situ density changes with X-ray diffractograms and Raman spectra of amorphous samples recovered at 77 K and 1 bar and show that the structural changes observable in recovered samples can be correlated with the pressure dependence of the in situ density values. We then discuss the density changes in the context of simulation studies reported recently.

The structural states of the amorphous ice forms have been named in recent publications in various ways and confusion can arise from that practice. We will restrict in the following the term HDA for the amorphous ice formed on compression of ice Ih at 77 K either under pressure or recovered at 1 bar,[1,2] and the term VHDA to the structural state obtained after isobaric annealing at $\geq \sim 0.8$ GPa and recovering at 77 K and 1 bar.[44] The structural states of amorphous ice obtained in situ on isobaric annealing at a given pressure we will call relaxed HDA (rHDA). The term rHDA has been used before for characterizing amorphous ice formed on annealing of HDA at 1 bar or in vacuo.[58,59] These forms of rHDA have densities lower than that of HDA whereas in our experiments rHDAs formed on annealing under pressure of ≥ 0.3

GPa have densities higher than that of HDA (cf. Fig. 2, later). We note the similar practice of Martoňàk et al.[39] in their simulation studies except that they used the term relaxed phase (RP) for the structural state annealed at a given pressure and subsequently cooled at this pressure to 80 K. It has also been proposed recently to characterize the various amorphous states, such as VHDA, by HDA with pressure and temperature added as suffix.[34] However, even that is not sufficient because time is also important for the structural state obtained at a given pressure and temperature (see refs. 31,60,61).

Experimental

The experiments were conducted with a piston cylinder apparatus using a pressure vessel with a bore of either 8 or 9 mm diameter and 60 mm length. The bore was lined with indium as described in ref. 62 and 63 to avoid pressure drops during compression. Pressurization was performed with a computerized "universal testing machine" (Zwick, Model BZ100/TL3S) at a controlled rate of 7000 N min^{-1}. The maximum pressure achieved was 1.9 GPa. Beyond that the piston started to deform. The positional reproducibility of the moving piston is ± 5 μm and the spatial resolution of the drive is 0.01 μm. Pressure calibration is described in detail in ref. 57. The accuracy of the given pressure values is expected to be below 0.04 GPa. Temperature was measured with a temperature sensor (Pt-100) inserted firmly in the piston cylinder apparatus. For slow heating the accuracy is estimated as ± 3 K, for rapid heating the error is expected to be slightly larger. Pressure–piston displacement curves served for the determination of the volume change and were recorded with the TestXpert V 7.1 Software of Zwick. The ΔV values during isobaric heating were calculated by multiplying the displacement of the testing machine's top crosshead with the area of the cross section of the piston cylinder. It is assumed that the diameter of the piston remains constant during the experiment. Furthermore, it is emphasized that the resulting ΔV functions do not only reflect the volume changes of the sample but also of every other part between moving top crosshead and fixed bottom crosshead.

With regard to the sample, 0.3000 cm^3 (0.5500 cm^3) of deionised water (H$_2$O) was pipetted (Gilson Pipetman, model P1000) into the precooled vessel with a bore diameter of 8 mm (9 mm). The density of liquid H$_2$O water is 0.9982 g cm^{-3} at 20 °C, i.e., 0.3000 cm^{-3} (0.5500 cm^{-3}) correspond to 0.2995 g (0.5490 g).

In a first experiment HDA was made by compression of ice Ih at 77 K up to 1.6 GPa (1.4 GPa). The pressure–displacement curves obtained had the same shape as those reported e.g. by Mishima et al.,[1,2] and as those shown in ref. 62 and 64, with a pronounced decrease in volume on compression above a nominal pressure of ~ 1.1 GPa due to the transition of ice Ih to HDA. HDA recovered after decompression under liquid N$_2$ at 1 bar was characterized by X-ray diffraction and its diffractogram is that reported in the literature,[1,2,24,40,62,64] with the maximum of the intense broad peak at 3.0 Å (cf. diffractogram (1) in Fig. 6(a), later).

In subsequent experiments HDA was made by compression of ice Ih at 77 K as described above. After decompression

This journal is © the Owner Societies 2006

Phys. Chem. Chem. Phys., 2006, 8, 386–397 | 387
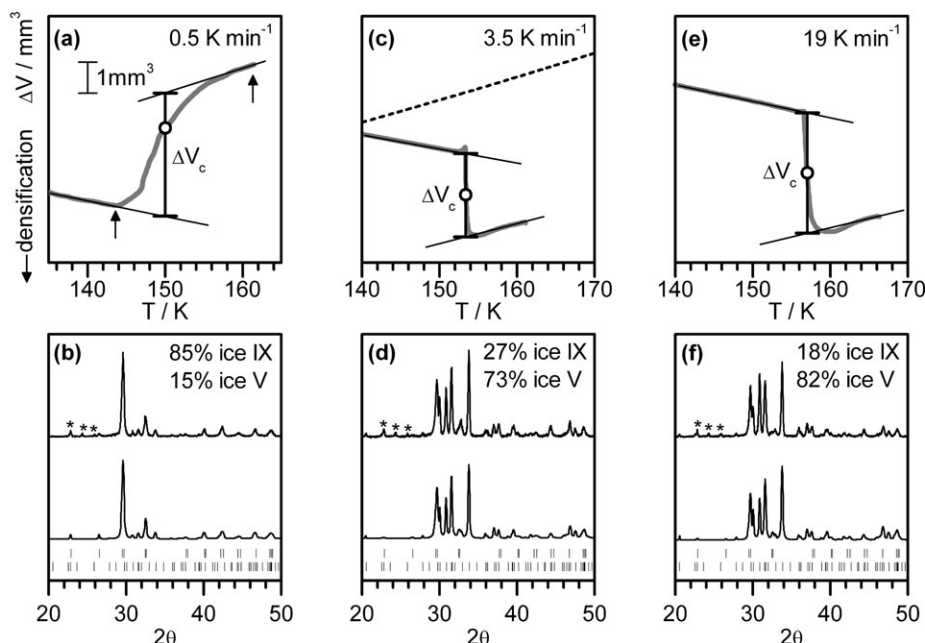
p=0.51 GPa

Fig. 1 Isobaric crystallization of HDA on heating at 0.51 GPa starting from 77 K. (a), (c) and (e) show the ΔV *versus* temperature curves (thick grey lines) obtained on heating at ~ 0.5 (a), ~ 3.5 (c) and ~ 19 (e) K min^{-1}; (b), (d) and (f) the X-ray diffractograms (Cu Kα) of the corresponding recovered samples (top), calculated diffractograms (bottom), weight fractions resulting from quantitative phase analysis and tickmarks for the reflection positions. Weight fractions and tickmarks of the different phases are given in the same order from top to bottom. Asterisks denote ice Ih impurity by condensed water vapour. The volume changes for the crystallization of HDA (ΔV_c) are determined by extrapolation (thin black lines) to the midpoint temperature of the transition and are indicated by thick black bars in (a), (c) and (e). The ordinate bar in (a) indicates a ΔV value of 1 mm^3, and the same bar holds for (c) and (e). Data from an isobaric heating experiment without ice sample at 0.51 GPa and a heating rate of ~ 3.5 K min^{-1} is shown as dashed black curve in (c). (Figure is adapted from Fig. 2 in ref. 57).

at 77 K to ambient pressure, the HDA samples were compressed again to certain pressures in the range from 0.21 GPa to 1.91 GPa and then heated isobarically without characterizing them by X-ray diffraction.

ΔV *versus* T plots presented in Fig. 1 show only the temperature range of crystallization. Monitored heating at a slow rate was started at ~ 110 K whereas faster heating was started at ~ 80 K.

X-ray diffractograms (Cu Kα) of samples recovered at 77 K and 1 bar were recorded at ~ 90 K on a diffractometer in θ–θ geometry (Siemens, model D 5000), equipped with a low-temperature camera of Paar. Diffractograms of crystalline samples were recorded with step size = 0.020° and step time = 1 s. For amorphous samples, however, step size = 0.050° and step time = 2.5 s was used. The sample plate was in horizontal position during the whole measurement. Installation of a "Goebel mirror" allowed us to use small amounts of sample without distortion of Bragg peaks. Analysis of the recorded X-ray diffractograms was performed with the "PowderCell" software (Version 2.4, BAM, Bundesanstalt für Materialforschung, Berlin, Germany). The weight fraction of high-pressure ices in the recovered crystallized mixtures was determined by quantitative phase analysis (QPA), using the Rietveld method.[65] Refined parameters included individual scale factors, lattice constants of the different phases, background coefficients, zero shift and profile parameters (Pseudo-Voigt2 profile functions). The error of the calculated weight fractions is estimated as

$\sim \pm 3\%$. The structural data of the various ice polymorphs were taken from refs. 66–76. Ice Ih reflections originating from condensation of water vapour onto the precooled sample plate holder (marked by asterisks, *cf.* ref. 57 for details) were excluded during the refinement procedure.

Raman spectra were recorded on a Labram-1B spectrometer equipped with a microscope (from Dilor company), through an ULWD-50 objective (Olympus company), by coadding four sets of spectra. A 20 mW He–Ne laser (632.8 nm) was used and the 1800 L/mm grating provides a resolution starting from 1.1 cm^{-1} at 150 cm^{-1} up to 0.6 cm^{-1} at 3600 cm^{-1}. The abscissa was calibrated with a silicon standard and the sharp Raman shifts are accurate to ± 2 cm^{-1}. An Oxford Microstat was used as cryostat. Temperature of the sample was controlled by a LakeShore CI330 autotuning temperature controller and remained constant within ± 0.2 K. Spectra were recorded at ~ 10 mbar and 80 K. For recording decoupled O–D stretching transitions, a solution of 5.0 wt% D$_2$O (from Aldrich, No. 15,188-2, 99.9 atom% D) in deionised H$_2$O water was used for the experiments. The resulting concentration of HOD in H$_2$O is 9.0 mol%.

Results

In situ density values on isobaric annealing

We first show in Fig. 1 how *in situ* density values of amorphous samples obtained on isobaric annealing are calculated

from the densities of the crystalline high-pressure ice phases and the change in volume (ΔV_c) on crystallization. This is shown exemplarily for the density of rHDA (ρ_{rHDA}) for an annealing pressure of 0.51 GPa: Fig. 1(a) shows ΔV on isobaric heating of HDA at ~ 0.5 K min^{-1} and 0.51 GPa (thick grey curve). Pronounced increase in volume starts at ~ 144 K (marked by arrow), indicating the crystallization to a less dense phase and it ends at ~ 157 K. Thereafter, the linear expansion of the crystallized mixture is observed. After heating to 162 K (marked by arrow) the sample was cooled at constant pressure of 0.51 GPa with liquid N$_2$ to 77 K at a rate of ~ 30–40 K min^{-1} and recovered under liquid N$_2$ at 1 bar. Thereafter it was quantitatively characterized by its X-ray diffractogram (cf. Fig. 1(b), top) as a mixture of 85% ice IX and 15% ice V, by simulating the diffractogram (cf. Fig. 1(b), bottom). A small amount of ice Ih is marked by asterisks in this and the following diffractograms. This ice Ih originates from condensation of water vapour during transfer of the sample onto the precooled sample plate holder of the diffractometer (cf. ref. 57 for details).

When the heating rate is increased to ~ 3.5 K min^{-1} (Fig. 1(c)), the onset of crystallization is shifted to higher temperature, to 152 K, and, after a weak ΔV increase, ΔV decreases drastically. The recovered sample consists of 27% ice IX and 73% ice V (Fig. 1(d)). On further increase of the heating rate to ~ 19 K min^{-1} (Fig. 1(e)), the onset of crystallization is found at even higher temperature, at 156 K and abrupt crystallization occurs with a sudden ΔV decrease. The recovered sample consists of 18% ice IX and 82% ice V (Fig. 1(f)). Ice V is more dense than ice IX.[66,70] Therefore, the ΔV increase of Fig. 1(a) is attributed to dominant formation of less dense ice IX, whereas the ΔV decrease of Fig. 1(e) is caused by dominant formation of more dense ice V. Detailed descriptions of the crystallization behaviour of HDA as a function of pressure and heating rate are given in ref. 57 and 77.

For the determination of the volume change for the crystallization of rHDA (ΔV_c), the linear gradients before and after crystallization are extrapolated to higher or lower temperatures, respectively (indicated by thin black lines in Fig. 1(a), (c), (e)). At approximately the midpoint temperature of the crystallization (T_c), ΔV_c corresponds to the vertical distance between the two extrapolated lines (indicated by thick black bars in Fig. 1(a), (c) and (e)).

By determining ΔV_c this way we circumvent the obstacle of unknown apparatus function since ΔV_c is determined by extrapolation to a certain temperature T_c. It is assumed that the apparatus function is linear within the relatively narrow temperature range of crystallization. This assumption is supported by the dashed curve in Fig. 1(c) which shows an isobaric heating experiment without HDA sample at 3.5 K min^{-1} and 0.5 GPa. Also the calculated densities shown below strongly support this view. ΔV_c values determined from Fig. 1(a), 1(c) and 1(e) are $+3.991$ mm^3 ($T_c = 150$ K), -2.707 mm^3 ($T_c = 153$ K) and -3.922 mm^3 ($T_c = 157$ K).

In a next step the densities of the various crystalline phases of ice were calculated at pressures and temperatures p_c and T_c when crystallisation occurred. To this aim the most reliable reported values obtained at conditions p_0 and T_0 (obtained by neutron diffraction, see Table 11.2 in ref. 66) where taken as

reference points and then corrected for the difference between p_c and p_0 as well as T_c and T_0. For this purpose, reasonable values of the thermal expansion coefficients α and bulk moduli B had to be assumed. Except for ice Ih a pressure-independent value of $\alpha = 1.6 \times 10^{-4}$ K^{-1} was used, as supported by measurements (cf. ref. 78 and references therein) and values of bulk moduli B were taken mostly from ultrasonic measurements[79] and empirically corrected for (small) temperature effects. For ice Ih accurate values of α are known[66] and B at low temperatures was determined by our own recent neutron diffraction measurements.[80] Given these values of α, B and the reference densities at p_0/T_0, the densities (ρ) at the crystallisation conditions p/T_c can be calculated by use of a simple Murnaghan equation of state (with $B' = 4$):[81]

$$\rho = \rho_0 \left(1 + \frac{B'}{B} p \right)^{1/B'} \qquad (1)$$

The density of a mixture of crystalline phases (ρ_{CM}) can then be determined using eqn (2) with the density values of the different phases (ρ_i) at a certain temperature (T_c) and pressure (p) and the weight fractions of the different crystalline phases in a mixture (w_i).

$$\rho_{CM}(T_c,p) = \frac{1}{\sum_i w_i / \rho_i(T_c,p)} \qquad (2)$$

With the weight fractions from quantitative phase analysis (cf. Fig. 1(b), (d) and (f)), the resulting ρ_{CM} values at 0.51 GPa are 1.227 g cm^{-3} ($T_c = 150$ K), 1.266 g cm^{-3} ($T_c = 153$ K) and 1.271 g cm^{-3} ($T_c = 157$ K).

The volume of a mixture of crystalline phases (V_{CM}) at a certain pressure and temperature is calculated next: The mass of the sample (m) is known from the volume of water which was pipetted into the piston apparatus at the beginning of the experiment. In case of the experiments described in Fig. 1, 0.2995 g of sample were used. The volume of rHDA at the crystallization (V_{rHDA}) can then be calculated from eqn (3) by subtracting ΔV_c from V_{CM}.

$$V_{rHDA}(T_c,p) = V_{CM}(T_c,p) - \Delta V_c(T_c,p) \qquad (3)$$

Applying this equation to the experiments shown in Fig. 1, we obtain $V_{rHDA}(150$ K, 0.51 GPa$) = 0.2401$ cm^3, $V_{rHDA}(153$ K, 0.51 GPa$) = 0.2393$ cm^3 and $V_{rHDA}(157$ K, 0.51 GPa$) = 0.2395$ cm^3. The density of rHDA (ρ_{rHDA}) at 0.51 GPa calculated from the three V_{rHDA} values is hence 1.25 g cm^{-3}. These density values are listed in Table 1.

We emphasize that the resulting densities agree very well, even though the calculations started from different compositions of the crystalline mixtures and the temperature interval decreased markedly with increasing heating rate (cf. Fig 1(a), (c) and (d)). Furthermore, the density values do not depend on whether less dense crystalline ice phases are formed as in (a), or more dense phases as in (c) and (e). Summarizing, this is convincing evidence that the effect of the apparatus function is negligible in these calculations.

Fig. 2 shows calculated ρ_{rHDA} values not only at 0.51 GPa but also at other pressures in the pressure range from 0.2 to 1.9 GPa (30 values indicated by diamonds, listed in Table 1). Some of the corresponding crystallization experiments are

This journal is © the Owner Societies 2006

Phys. Chem. Chem. Phys., 2006, 8, 386–397 | 389
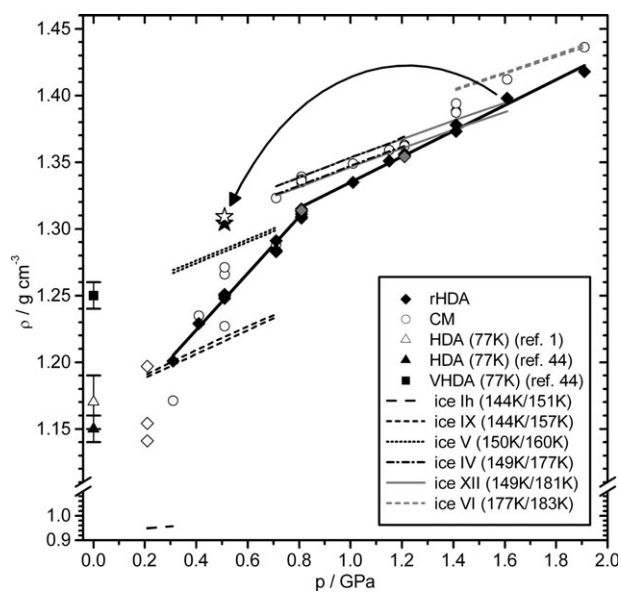
Fig. 2 Calculated density values of rHDA (ρ_{rHDA}) in the pressure range 0.2 to 1.9 GPa (30 data points indicated by diamonds). Data points indicated by full (grey) diamonds originate from experiments with a 8 mm (9 mm) pressure vessel and 0.2995 g (0.5490 g) sample mass. Data values at 0.2 GPa (open diamonds) exhibit a relatively large error (see Results section for further details). Linear fits of ρ_{rHDA} below and above 0.8 GPa are indicated by thick black lines with gradients of 0.21 g cm^{-3} GPa^{-1} below 0.8 GPa and 0.10 g cm^{-3} GPa^{-1} above 0.8 GPa. Densities of the different crystalline mixtures (CM), obtained after complete crystallization of the amorphous samples, are indicated by open circles. The isotherms of the different crystalline phases are shown as lines. In one experiment, HDA was first heated isobarically at 1.61 GPa to a temperature ∼5 K below the onset temperature of crystallization, then quenched to 77 K, reheated isobarically at 0.51 GPa (indicated by arrow) and finally allowed to crystallize. The density of the amorphous sample at the crystallization and the density of the crystallized phase is indicated by a full and open star, respectively. Density values of HDA and VHDA at 77 K and 1 bar from ref. 44 are depicted by a full triangle and a full square, respectively. Mishima *et al.*'s density value of HDA at 77 K and 1 bar is shown by an open triangle.[1]

Table 1 Calculated densities of rHDA (ρ_{rHDA}) at the given annealing pressures (p_A) and mid-point temperatures of the crystallization (T_c). Density values marked with asterisks (*) originate from experiments with a 9 mm diameter pressure vessel and 0.5490 g sample mass. All other experiments were performed using a 8 mm diameter pressure vessel and 0.2995 g sample mass. In one experiment, HDA was first heated isobarically at 1.61 GPa to a temperature ∼5 K below the onset temperature of crystallization, then quenched to 77 K, reheated isobarically at 0.51 GPa, and finally allowed to crystallize. The density of this amorphous sample at the crystallization is indicated by a cross (+)

p_A/GPa	T_c/K	ρ_{rHDA}/g cm^{-3}
0.31	151	1.20
0.41	153	1.23
0.51	150	1.25
0.51	153	1.25
0.51	157	1.25
0.71	151	1.28
0.71	151	1.28
0.71	160	1.29
0.81	149	1.31
0.81	149	1.31
0.81	158	1.31
0.81	160	1.31*
0.81	164	1.31
0.81	165	1.32
0.81	168	1.31
0.81	168	1.31
1.01	170	1.34
1.17	173	1.35
1.21	172	1.35
1.21	173	1.36
1.21	175	1.35
1.21	176	1.35*
1.21	177	1.36
1.41	177	1.38
1.41	177	1.37
1.61	181	1.40
1.91	183	1.42
0.51	150	1.31+

shown in ref. 57 in Fig. 1–6. Most values were calculated from data using a 8 mm diameter bore vessel and 0.2995 g sample mass. However, two values at 0.81 and 1.21 GPa (grey diamonds) originate from experiments with a 9 mm diameter pressure vessel and 0.5490 g sample mass. The densities obtained with the 9 mm vessel are in very good agreement with the other data which therefore demonstrates the independence of the calculated density values from sample mass and diameter of the pressure vessel's bore.

The density values at 0.21 GPa are drawn as open diamonds and show quite large errors compared to the other values. At 0.21 GPa, rHDA crystallizes to ice Ih and ice IX with their weight fractions depending systematically on the heating rate.[57] The comparatively large error of the calculated densities at 0.21 GPa arises from the fact that water vapour condenses onto the sample during transfer of the sample into the precooled sample holder forming ice Ih which does not originate from the crystallization of rHDA (*cf.* ref. 57 for details). The determined weight fractions of ice Ih are there-

fore slightly too large (5–10%). In addition, the difference in density between ices Ih and IX is relatively large. This means that the calculation of the rHDA density depends sensitively on the weight fraction of ice Ih and consequently a slight error in the weight fractions of ice Ih has a large influence on the resulting density of rHDA. Contrary to that, an error in the weight fraction of *e.g.* ice IV in a mixture of ices IV and XII would have almost no influence on the calculated density of rHDA since ices IV and XII have very similar densities. Because of these issues, the density values obtained at 0.2 GPa are not included in the calculation of the slope.

The bulk densities of the different crystalline mixtures under pressure (ρ_{CM}) are indicated by open circles. The isotherms of the different crystalline phases are depicted as lines. For each phase, the isotherms of the lowest and highest T_c, which are needed for the calculation of ρ_{rHDA}, are shown (see legend of Fig. 2 for further details).

The calculated densities of rHDA exhibit a pronounced change of slope at approximately 0.8 GPa with a slope of 0.21 g cm^{-3} GPa^{-1} below 0.8 GPa and a slope of 0.10 g cm^{-3} GPa^{-1} above 0.8 GPa.

In one experiment, HDA was heated isobarically to 170 K at 1.61 GPa (5 K below onset of crystallization at a heating

rate of ∼3 K min⁻¹, *cf.* Fig. 8 in ref. 57), then quenched to 77 K and finally reheated at 0.51 GPa (indicated by arrow) and allowed to crystallize. The density of this sample at the crystallization temperature and the density of the crystallized mixture are indicated by a full star and a open star, respectively. The composition of the recovered sample is: 19% ice V, 7% ice IV and 74% ice XII. It is important to note that this composition differs from that obtained on crystallizing HDA at 0.5 GPa (*cf.* Fig. 1). Instead, ice IV and ice XII are formed only above 0.5 GPa.[57]

Density values of HDA and VHDA at ambient pressure and 77 K from ref. 44 are indicated by a full triangle and full square. Mishima *et al.*'s density value of HDA at 77 K is shown as an open triangle.[1]

The T_c values of all crystallization experiments are shown in Fig. 3(a). Variations in T_c at a given pressure originate from the use of different heating rates (*cf.* ref. 57). Most density values were obtained from crystallization experiments at 0.51, 0.81 and 1.21 GPa. Fig. 3(b) shows therefore ρ_{rHDA} as a function of T_c at 0.51 GPa (squares), 0.81 GPa (diamonds) and 1.21 GPa (triangles). Grey symbols indicate again the use of a 9 mm piston cylinder and 0.5490 g sample mass. Significant changes of ρ_{rHDA} as a function of temperature could not be observed at any of the pressures.

Raman spectra of recovered amorphous ice samples

The relaxation process from HDA to rHDA was investigated at 0.51 and 1.17 GPa. HDA samples were heated isobarically
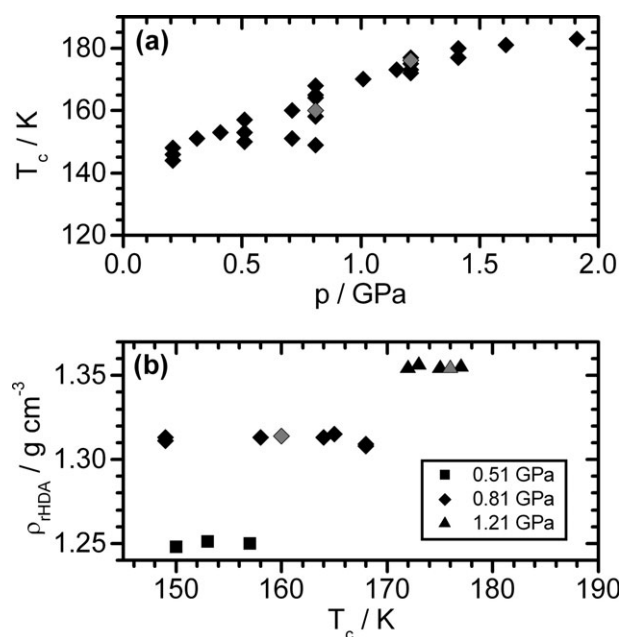
Fig. 3 (a) Midpoint temperatures (T_c) of the different crystallization experiments used for the calculation of the density values of rHDA (ρ_{rHDA}). Variations in T_c at a given pressure originate from different heating rates (*cf.* ref. 57 for further details). (b) ρ_{rHDA} plotted against T_c at pressures of 0.51 GPa (squares), 0.81 GPa (diamonds) and 1.21 GPa (triangles). Full (grey) data points in (a) and (b) originate from experiments with a 8 mm (9 mm) pressure vessel and 0.2995 g (0.5490 g) sample mass.

at ∼3 K min⁻¹ to a set of annealing temperatures (T_A) between 77 K and ∼5 K below the onset temperature of crystallization which is 165 K at 1.17 GPa and 152 K at 0.51 GPa (*cf.* ref. 57). After reaching T_A, the samples were immediately quenched to 77 K, decompressed to ambient pressure and characterized by Raman spectroscopy at 80 K and 10 mbar. Fig. 4(a) and (c) show spectra of the coupled O–H stretching transition (ν(OH)) of samples annealed at 1.17 GPa and 0.51 GPa, respectively. The decoupled O–D stretching transition (ν(OD)) of samples annealed at 0.51 GPa are shown in (e). The peak positions of the spectra in (a), (c) and (e) are plotted together with additional data in (b) (p_A = 1.17 GPa), (d) (p_A = 0.51 GPa) and (f) (p_A = 0.51 GPa) against T_A. In one experiment at 1.17 GPa the sample was heated to 153 K and kept isothermally for 6 hours before quenching (*cf.* (a)). The corresponding ν(OH) peak position is indicated by a star in (b). The relaxation process from HDA to rHDA is clearly visible as a sudden pronounced change in the peak positions of the coupled O–H (b, d) and the decoupled O–D stretching transition (f). The largest changes in the peak positions occur between 121 and 130 K at 1.17 GPa and between 100 and 116 K at 0.51 GPa. Annealing at temperatures higher than 130 K at 1.17 GPa and 116 K at 0.51 GPa has no influence on the peak positions within the experimental error. The temperature range of crystallization is indicated by grey shaded areas in (b), (d) and (f).

In a separate set of experiments (not shown), HDA samples were heated at 1.17 GPa to certain temperatures below crystallization, quenched and then heated again. On reaching the temperatures before quenching, ΔV values became identical with the ΔV values of the first heating. This indicates that irreversible density changes do not occur during quenching and that the spectra of the quenched samples are representative for those of the warmer samples before quenching.

Fig. 5 shows the Raman spectra of recovered rHDA samples as a function of the annealing pressure (p_A) in the pressure range from 0.31 to 1.61 GPa. The HDA samples were first heated isobarically from 77 K to ∼5 K below the onset-temperature of crystallization at ∼3 K min⁻¹, then quenched to 77 K, decompressed to ambient pressure and characterized. T_A was 136 K at 0.31 GPa, 146 K at 0.51 GPa, 152 K at 0.81 GPa, 161 K at 1.17 GPa and 170 K at 1.61 GPa. The coupled O–H stretching transitions (ν(OH)) and decoupled O–D stretching transitions (ν(OD)) of the recovered samples are shown in (a) and (c), respectively. The corresponding peak positions of the spectra in (a) and (c) are plotted in (b) and (d) *versus* p_A, together with additional data. The peak positions of the coupled O–H and decoupled O–D stretching transition of (not annealed) HDA are indicated by dotted lines in (b) and (d). The changes in the peak positions for both ν(OH) and ν(OD) are comparatively large between p_A = 0.31 and 0.81 GPa. Above 0.81 GPa, ν(OH) and ν(OD) seem to level off slightly.

X-ray diffractograms of recovered amorphous ice samples

The above obtained recovered rHDA samples were additionally probed by using X-ray diffraction. Fig. 6(a) shows the X-ray diffractograms of HDA as-prepared by compression of ice Ih at 77 K (1) and of recovered rHDA samples annealed at

This journal is © the Owner Societies 2006

Phys. Chem. Chem. Phys., 2006, **8**, 386–397 | **391**
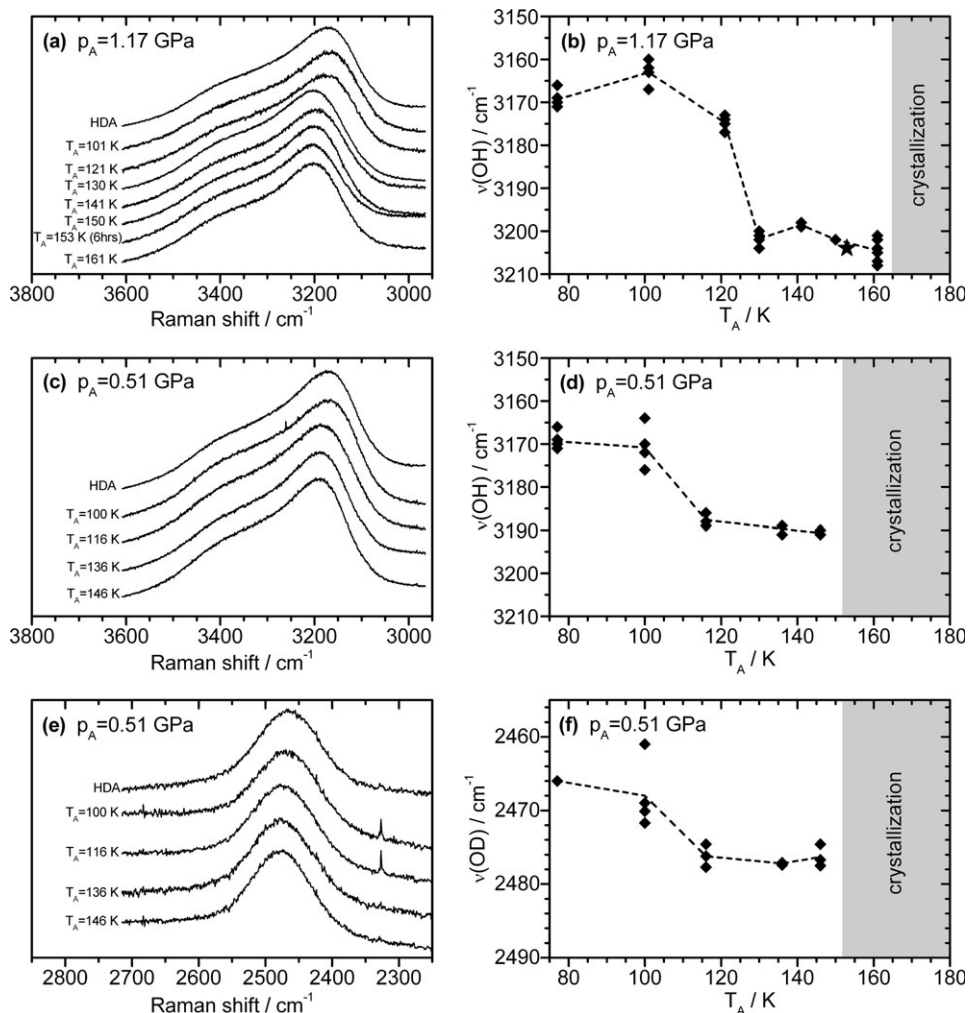
Fig. 4 Raman spectra ($\lambda_0 = 632.8$ nm) of recovered (r)HDA samples as a function of the annealing temperature (T_A) at annealing pressures (p_A) of 0.51 and 1.17 GPa. Spectra were recorded at 80 K and 10 mbar. (a) and (c) show spectra of the coupled O–H stretching transition (ν(OH)) of samples annealed at 1.17 GPa and 0.51 GPa, respectively. The decoupled O–D stretching transition (ν(OD)) of samples annealed at 0.51 GPa are shown in (e). Spectra in (a), (c) and (e) were scaled to approximately same peak intensities and shifted vertically for clarity. Peak positions of the spectra in (a), (c) and (e) are plotted together with additional data in (b) ($p_A = 1.17$ GPa), (d) ($p_A = 0.51$ GPa) and (f) ($p_A = 0.51$ GPa) against T_A. T_A and p_A are indicated for each spectrum. In one experiment at 1.17 GPa the temperature was kept isothermally at 153 K for 6 hrs before quenching (*cf.* (a)). The corresponding peak position of the coupled O–H stretching transition is indicated by a star in (b). Crystallization of the amorphous sample is indicated by grey shadowed areas in (b), (d) and (f). In Fig. 4–6, data points are connected by lines for clarity.

136 K and 0.31 GPa (2), 146 K and 0.51 GPa (3), 152 K and 0.81 GPa (4), 161 K and 1.17 GPa (5) and at 170 K and 1.61 GPa (6). The X-ray diffractograms are shown as functions of 2θ. The top axis of Fig. 6(a) shows the corresponding d-spacings. Tickmarks indicate the reflection positions of ice Ih, which originates from vapour condensation onto the sample holder (*cf.* above). The X-ray diffractograms were analysed to determine peak maximum and "full width at half height" (fwhh) of the strongest broad diffraction peak. Fig. 6(b) shows the peak maxima (full diamonds) and fwhh's (open circles) as a function of annealing pressure (p_A). Peak position and fwhh of pristine HDA ((1) in Fig. 6(a)) can not be assigned to a certain annealing pressure. Therefore they are indicated by a solid and a dashed horizontal line, respectively. The largest changes with respect to peak position and fwhh are observed between $p_A = 0.51$ and 1.17 GPa.

Discussion

The main error for calculating densities from ΔV changes in piston cylinder experiments is that the sample contains cracks and/or voids and that these change with temperature by macroscopic densification (pressure consolidation). This error is minimized here because the ΔV change in a *small* temperature region, the region of crystallization, is used for the calculation of the density values. Thus, the *in situ* density values reported here are more reliable than our previous density estimations at 170 K at 1.1 and 1.9 GPa which were based on the total ΔV decrease from 77 to 170 K.[44] In fact, the previously reported density values would require crystallization of rHDA at 1.1 and 1.9 GPa to *less* dense crystalline phases which is not observed for pressures higher than 0.7 GPa.[57] We are confident that the problematic effect of the apparatus function in piston cylinder
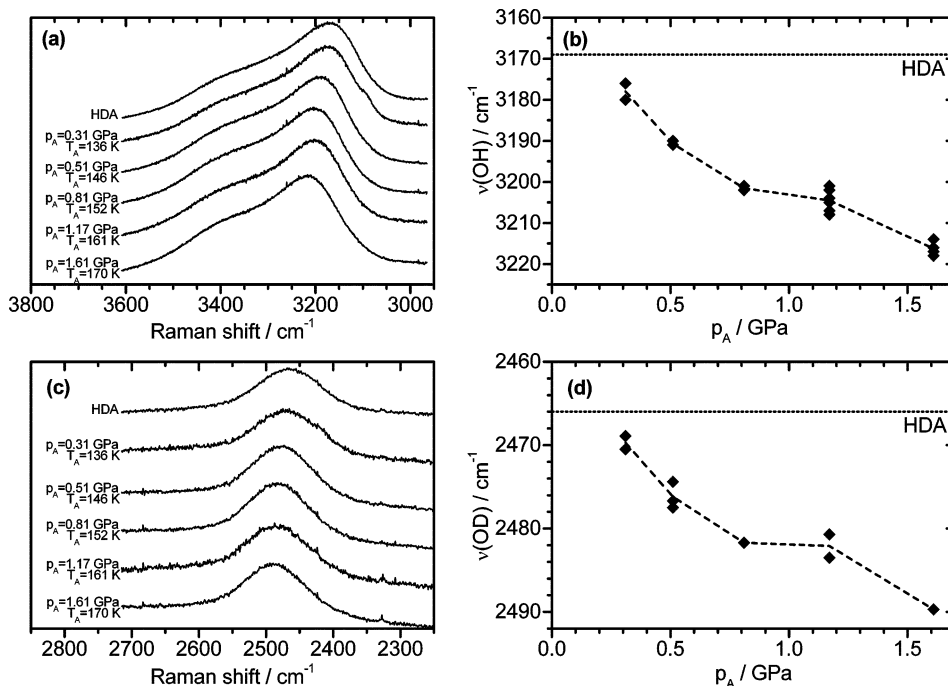
Fig. 5 Raman spectra (λ_0 = 632.8 nm) of recovered rHDA samples recorded at 80 K and 10 mbar. Coupled O–H stretching transitions (ν(OH)) and decoupled O–D stretching transitions (ν(OD)) are shown in (a) and (c), respectively. Spectra in (a) and (c) were scaled to approximately same peak intensities and shifted vertically for clarity. T_A and p_A are indicated for each spectrum. Peak positions of the spectra in (a) and (c) are plotted together with additional data in (b) and (d) against the annealing pressure (p_A). The peak positions of the coupled O–H and decoupled O–D stretching transition of (not annealed) HDA are indicated by dotted lines in (b) and (d).

experiments can be eliminated by using the above described extrapolation procedure. This is strongly supported by the fact that density values obtained at a given pressure are identical within experimental error for widely different heating rates, temperature regions of crystallization, different sample mass, pressure vessel and different compositions of the crystallized material (*cf.* Fig. 1–3).

Our approach further presupposes that the composition of ice phases formed on crystallization of rHDA does not change on quenching the sample to 77 K and recovering at 1 bar, or on heating up to *e.g.* 162 K as in Fig. 1(a). For the experiment shown in Fig. 1, the stable phase at 0.5 GPa is ice II.[66] We emphasize that none of the recovered ice phase mixtures studied here or in ref. 57 contained any ice II reflections. Thus, the stable ice II phase does not form at the low temperatures of this study. Furthermore, *in situ* neutron diffraction studies of ice III/IX and of ice V showed no evidence for ice III/IX transforming into ice V or *vice versa*,[70,72] and thus, the recovered fractions of ice IX/ice V in Fig. 1 are the same as those after crystallization, or as that on heating up to 162 K (Fig. 1(a)). We further ruled out in ref. 64 for crystallization of rHDA at 0.8 GPa that ice IV transforms into ice XII (*cf.* Fig. 1(c) and (g)). These results are consistent with the general notion that quenched and recovered high-pressure ice phases are expected to be the same as those formed under pressure whenever restructuring of the oxygen positions is involved because this is too slow at low temperatures.[66]

The data for the amorphous ice density *versus p* plot in Fig. 2 are not and cannot be, determined under isothermal conditions because T_c (the midpoint temperature of crystallization)

increases with increasing p (*cf.* Fig. 3(a)) and a small temperature region is necessary for each data point in order to determine the ΔV change from the temperature region of crystallization. Nevertheless, the effect of temperature on the density value is minor or negligible in comparison to that of pressure because, as shown in Fig. 3(b), T_c can change by up to $\sim$20 K at a given pressure by varying the heating rate but the density remains either constant (1.36 g cm^{-3} at 1.21 GPa and 1.25 g cm^{-3} at 0.51 GPa) or it changes only by a small amount (from 1.31 to 1.30 g cm^{-3} at 0.81 GPa).

The prominent feature in the amorphous ice density *versus p* plot (Fig. 2) is the pronounced change of slope at $\sim$0.8 GPa, with a slope of 0.21 g cm^{-3} GPa^{-1} below 0.8 GPa and of 0.10 g cm^{-3} GPa^{-1} above 0.8 GPa. This implies that the densification mechanism between 0.3 and 0.8 GPa reaches a limit at $\sim$0.8 GPa and that further densification above $\sim$0.8 GPa occurs by another mechanism.

Raman spectra of recovered samples

Raman spectra of recovered samples indicate the temperature region where relaxation occurs on isobaric heating at pressures of 0.51 and 1.17 GPa (*cf.* Fig. 4). The first set of data in Fig. 4 obtained from HDA samples annealed at 1.17 GPa (Fig. 4(a)) shows a stepwise change in the peak position with increasing T_A (Fig. 4(b)): no change in ν(OH) on heating from 77 K up to 101 K, a slight increase by $\sim$5 cm^{-1} on increasing T_A up to 121 K, a drastic increase by $\sim$30 cm^{-1} on further increase of T_A up to 130 K and nearly constant peak maximum on further increasing T_A up to 161 K.

The peak maximum of the coupled O–H stretching band region (ν(OH), Fig. 4(c)) for $p_A = 0.51$ GPa is plotted in Fig. 4(d) *versus* the annealing temperature (T_A). This plot shows that at 0.51 GPa the peak maximum at $\sim$3170 cm^{-1} does not change on heating from 77 K up to 100 K, that it increases up to $\sim$3190 cm^{-1} on further heat treatment up to 116 K and remains nearly constant again on even further heating up to 146 K.

Fig. 4(e) further shows Raman spectra of the decoupled (OD) stretching transition of recovered samples recorded in the same manner. The plot of the peak maximum of the

decoupled OD stretching transition, ν(OD), *versus* T_A (Fig. 4(f)) shows that ν(OD) is at 2466 cm^{-1} at 77 K, does not change on heating from 77 to 100 K, increases by $\sim$10 cm^{-1} on further increase of T_A to 116 K and remains constant on further increase of T_A to 146 K.

The steps in both the coupled ν(OH) and the decoupled ν(OD) *versus* T_A plots indicate the temperature region where Raman spectra show an *irreversible* relaxation process from HDA to rHDA. This is between $\sim$100 and $\sim$116 K at 0.51 GPa (Fig. 4(d) and (f)) and between $\sim$121 and $\sim$130 K at 1.17 GPa (Fig. 4(b)). The Raman spectra of the recovered rHDA samples are generally, except for differences in peak positions, very similar to the spectrum of pristine HDA. The changes in peak frequency caused by the relaxation process are $\sim$10 cm^{-1} for ν(OD) at 0.51 GPa, $\sim$21 cm^{-1} for ν(OH) at 0.51 GPa and $\sim$35 cm^{-1} for ν(OH) at 1.17 GPa. The coupled ν(OH) stretching transition seems thus to be more sensitive for the structural changes occurring during relaxation than the decoupled ν(OD) stretching transition. However, it has been stated recently that the spectral features of coupled O–H bands are "difficult to correlate with structural details, either on a local length scale and even more so with the structural network on an intermediate (3–10 Å) or longer length scale".[59] Correlations between the decoupled O–D peak frequency and hydrogen-bonded average O–H···O distance allow obtaining an estimate of average O–H···O distances from the Raman spectrum. With the correlation reported in ref. 82 we obtain from the decoupled O–D peak frequencies of Fig. 4(e) and (f) average O–D···O distances of 2.820 Å for 77 K, of 2.823 Å for T_A of 100 K, of 2.836 Å for T_A of 116 K and of 2.838 Å for T_A of 136 K. Thus, the average O–D···O distance increases between T_A of 100 and 116 K by $\sim$0.013 Å and it remains nearly constant on further increase of T_A from 116 to 146 K.

It has been argued that the correlation reported in ref. 82 for estimation of average O–D···O distances from decoupled O–D peak frequencies has been developed from ice VII data and thus, should be used only for crystalline ice samples. However, Guthrie *et al.*[53] report O···O distances for HDA and VHDA from their X-ray data which are very similar to those calculated by Loerting *et al.*[44] from decoupled O–D Raman peak frequencies. Thus, the relation reported in ref. 82 seems to hold also for amorphous ice samples.

We conclude, that rHDA is fully relaxed above $\sim$116 K at 0.5 GPa and above $\sim$130 K at 1.2 GPa according to Raman spectra. This fact is particularly supported by one experiment where rHDA was annealed at $T_A = 153$ K and $p_A = 1.17$ GPa for 6 hours. The ν(OH) peak frequency of the recovered sample is indicated by a star in Fig. 4(b) and is identical within the experimental error with values of the other rHDA samples which were immediately quenched after reaching T_A. The complete relaxation of rHDA is also important with respect to the observed inflection in the density values of rHDA (*cf.* Fig. 2): If complete relaxation would not occur before crystallization, the observed inflection in the density values (*cf.* Fig. 2) could also be explained by crystallization from partially relaxed states below $\sim$0.8 GPa and fully relaxed states at higher pressures.

According to our Raman data, the relaxation temperature (T_R) increases with increasing pressure ($dT_R/dp > 0$). We
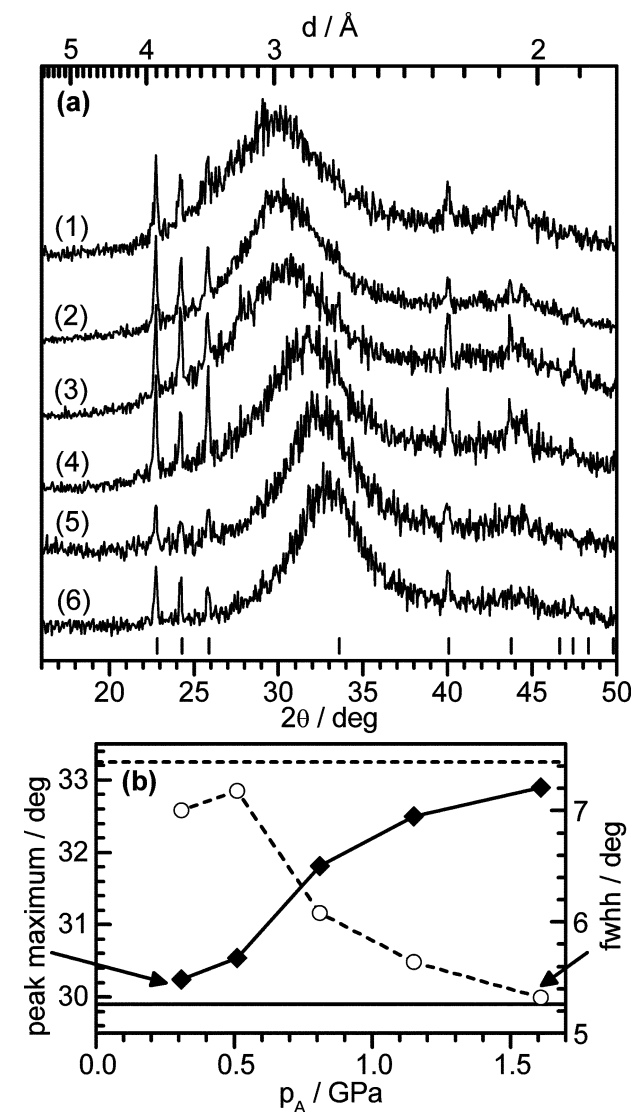
Fig. 6 X-ray diffractograms (Cu Kα) of recovered HDA and rHDA samples recorded at $\sim$90 K *in vacuo*. (a) Shows the diffractograms of HDA (1) and rHDA samples annealed at 0.31 GPa/136 K (2), at 0.51 GPa/146 K (3), at 0.81 GPa/152 K (4), at 1.17 GPa/161 K (5) and at 1.61 GPa/170 K (6). Tickmarks indicate the reflection positions of ice Ih which originates from condensation of water vapour onto the sample holder. Peak position ($\blacklozenge$) and "full width at half height" ($\bigcirc$) of the strongest diffraction peaks in diffractograms (1–6) are shown in (b) as a function of p_A. The peak position and fwhh of HDA are indicated by a solid and a dashed horizontal line, respectively.

interpret this finding in terms of slowing down of the relaxation kinetics as is expected for processes with positive activation volumes (*cf*. $dT_c/dp > 0$ in Fig. 3(a)). Therefore, the apparent increasing thermal stability of HDA with increasing pressure in the pressure range 0.5 to 1.2 GPa is assumed to have kinetic reasons.

The change of slope at $\sim$0.8 GPa in the density *versus* pressure plot (Fig. 2) is also observable in the ν(OH) and ν(OD) *versus* p_A plots (Fig. 5(b) and (d)). These peak positions were also obtained from Raman spectra of recovered samples (Fig. 5(a) and (c)), after isobaric heating and annealing. T_A was chosen such that according to Fig. 4 the rHDA's are fully relaxed for each pressure ($\sim$5 K below the onset-temperature of crystallization). ν(OH) increases with pressure starting from 3178 cm^{-1} at 0.31 GPa, 3191 cm^{-1} at 0.51 GPa, 3202 cm^{-1} at 0.81 GPa, 3205 cm^{-1} at 1.17 GPa to 3216 cm^{-1} at 1.61 GPa.

Fig. 5(d) shows that ν(OD) increases from 2469.7 cm^{-1} at 0.31 GPa, 2476.2 cm^{-1} at 0.51 GPa, 2481.7 cm^{-1} at 0.81 GPa, 2482.1 cm^{-1} at 1.17 GPa to 2489.7 cm^{-1} at 1.61 GPa. (The value at 1.17 GPa is about that reported by Loerting *et al.*[44] for VHDA.) Average O–D$\cdots$O distances calculated from ν(OD) values (Fig. 5(d)) according to ref. 82 are 2.826 Å (2469.7 cm^{-1}) for 0.31 GPa, 2.836 Å (2476.2 cm^{-1}) for 0.51 GPa, 2.846 Å (2481.7 cm^{-1}) for 0.81 GPa, 2.846 Å (2482.1 cm^{-1}) for 1.17 GPa and 2.860 Å (2489.7 cm^{-1}) for 1.61 GPa. The average O–D$\cdots$O distance seems thus to increase with increasing pressure, although the densities of the rHDA samples increase with increasing pressure (*cf*. Fig. 2). The general interpretation of this distance-pressure paradox is an increase of coordination number.[26]

X-ray diffractograms of recovered samples

When HDA is heated at 0.51 GPa up to 146 K and recovered subsequently at 77 K and 1 bar, its X-ray diffractogram shows a small shift of the maximum of the intense broad peak from 3.00 Å (2.989 Å in Fig. 6(a)(1)), the value reported for HDA without subsequent annealing,[1,2,24,40] to 2.929 Å (Fig. 6(a)(3)), but its fwhh remains about the same. Drastic changes in the X-ray diffractogam of the recovered sample occur after annealing at 0.81 GPa and heating up to 152 K (Fig. 6(a)(4)): the peak maximum shifts to 2.819 Å and the fwhh is reduced significantly. When p_A is increased further to 1.17 and 1.61 GPa, further changes in the diffractogram are observed: the peak maximum shifts to 2.761 Å for p_A = 1.17 GPa and 2.723 Å for p_A = 1.61 GPa. This goes along with small further decreases in fwhh.

These changes in the position and fwhh of the principal X-ray diffraction peak can be related to structural changes by following Guthrie *et al*'s[53] careful analysis of the X-ray and neutron structure factor functions ($S(Q)$) of recovered VHDA and their comparison with those of recovered HDA and LDA. They also observed the "increase in the peak position with increasing density and particularly the increase in the peak height and smaller peak width of the VHDA form relative to the HDA form. The periodicity of the short-intermediate range structure is inversely associated with the position of the principal peak position in $S(Q)$ and its width is often associated with the extent of ordering. The relative peak width indicates that ordering in the VHDA ice form is likely extended over a significantly longer range than that in the HDA ice form".[53] Thus, along these lines our X-ray diffractograms of recovered samples (Fig. 6) indicate that at 0.5 GPa the pressurized sample has still mainly the structural state of HDA, whereas at 0.81 GPa it has changed to that of more highly ordered VHDA.

We conclude that the inflection at $\sim$0.8 GPa (Fig. 2) seems to indicate the end of the pressure region where annealing leads to major structural changes in the rHDA's. X-ray diffractograms and Raman spectra of recovered samples agree in that structural changes on isobaric annealing are most pronounced for pressures between 0.3 and 0.8 GPa (compare Fig. 6(b) with Fig. 5(b) and (d)). However, these structural changes on p increase do not occur in the same manner: on p increase from 0.3 to 0.5 GPa, the peak maximum and fwhh of the main peak in the diffractograms barely changes and a pronounced change occurs only on further p increase to 0.8 GPa (Fig. 6(b)), whereas about half of the increase in ν(OH) and ν(OD) occurs already between 0.3 and 0.5 GPa. This could be due to the fact that X-ray diffractograms and Raman spectra probe different structural changes. Guthrie *et al.*[53] pointed out in their recent X-ray and neutron diffraction study that an important structural detail between HDA and VHDA is *increased intermediate* range structure and ordering in the latter. The notable features in our X-ray diffractograms of recovered samples (Fig. 6(a) and (b)) are increase in the peak position and decrease of the fwhh with increasing pressure and these features probe both short- and medium-range structural changes. However, ν(OD) values obtained from Raman spectra are correlated with average O–D$\cdots$O distances and this is considered an indirect measure of the local hydrogen bond length only.[59] Thus, by comparing the pressure dependence of structural changes in annealed and recovered samples by X-ray diffraction and Raman spectroscopy we can obtain a more detailed picture.

We propose that on annealing between $\sim$0.3 and $\sim$0.8 GPa mainly irreversible structural changes cause the pronounced increase of density with pressure, whereas on further increase of pressure from $\sim$0.8 to 1.9 GPa the less pronounced density increase is to a large extent elastic and reversible. This is consistent with an experiment where prior heating of HDA at a pressure of 1.6 GPa up to 170 K, that is $\sim$5 K below the onset temperature of crystallization, caused irreversible structural changes because after cooling and subsequent isobaric heating at 0.5 GPa above T_c the density is calculated as 1.31 g cm^{-3}. This value is much higher than the 1.25 g cm^{-3} value obtained from samples on first heating at 0.5 GPa (*cf*. Fig. 2, arrow, density value indicated by full star).

If the linear gradient between 0.8 and 1.9 GPa is extrapolated to 0.51 GPa, which means assuming perfectly reversible and elastic behaviour, this gives a density value of $\sim$1.29 g cm^{-3} at 0.51 GPa (*cf*. Fig. 2). The difference in density between 1.29 and 1.31 g cm^{-3} indicates that even above 0.8 GPa subtle irreversible changes take place. These structural changes between p_A = 0.81 and 1.61 GPa can also be seen clearly in the Raman spectra (*cf*. Fig. 5(b, d)) and the X-ray diffractograms of the recovered phases (*cf*. Fig. 6(b)). Recovered phases from the range of annealing pressures between 0.8 and 1.9 GPa were previously assumed to have the same

This journal is © the Owner Societies 2006

Phys. Chem. Chem. Phys., 2006, **8**, 386–397 | 395

structure, that of VHDA.[44] Further evidence for subtle structural changes in the rHDAs between 0.8 and 1.9 GPa other than reversible and elastic compression can be seen in Fig. 2: Although the slope of the density *versus p* decreases considerably above ∼0.8 GPa, it is still steeper than those of the crystalline phases in the same pressure range (ices IV, XII and VI) which are expected to show elastic compression only. However, taking into account the major structural changes between 0.3 GPa and 0.8 GPa and the only subtle changes above 0.8 GPa, we propose to call the rHDA states above ∼0.8 GPa VHDA. (Although Loerting *et al.*[44] defined the VHDA state originally for 77 K and ambient pressure, the assignment to the states under pressure has already been made in the literature.) Considering the subtle structural changes above 0.8 GPa, it would be most accurate to call the rHDA states above 0.8 GPa VHDA's and give additionally the annealing pressure.

Extrapolation of the linear gradient of the ρ_{rHDA} values between 0.8 and 1.9 GPa to 0 GPa gives a density of 1.23 g cm^{-3}. This agrees closely with the VHDA value of 1.25 g cm^{-3} (Fig. 2, full square) determined by buoyancy at 77 K and ambient pressure.[44] When we further consider the difference in temperature (144–183 K for the ρ_{rHDA} values in Fig. 2 *versus* 77 K for recovered VHDA), the extrapolated value of 1.23 g cm^{-3} is expected to be slightly higher and even closer to that of recovered VHDA.

We emphasize that density changes of rHDA between 1.6 and 1.9 GPa become even smaller than those between 0.8 and 1.6 GPa (*cf.* Fig. 2) and that in this pressure range the density differences between rHDA and the ice VI isotherm seem to remain basically constant. Thus, the compression of rHDA is expected to become perfectly reversible and elastic at pressures higher than 1.9 GPa which would be the ultimate definition for the VHDA state.

Comparison with simulation studies

We next attempt to relate our experimental data to those obtained by simulations. Of the several simulation studies of VHDA, those of Martoňák *et al.*[38,39] follow most detailed the experimental approach of Loerting *et al.*[44] They reported results of molecular dynamics simulations where HDA, made by compression of ice Ih at 80 K, is isobarically annealed at pressures up to 2.25 GPa and T_A of 170 K in order to generate relaxed states. They confirm the existence of experimentally observed phenomena, namely of VHDA[44] and of a continuum of HDA forms,[58,59] and they suggest that both phenomena originate from a relation between the density and the topology of the hydrogen-bonded network. By comparison of simulated O–O rdf's with that of VHDA recovered at 77 K and 1 bar,[46] they established that a continuum of HDA states forms at pressures between ∼0.2–0.9 GPa and VHDA forms above 0.9 GPa (ref. 38) or 1.0 GPa.[39]

Martoňàk *et al.*'s[38,39] detailed analysis of the network structure in terms of the shapes of hydrogen-bonded rings reveals that substantial reconstruction of the topology of the hydrogen bonded network and changes in the ring statistics from *e.g.* mainly six-membered to mainly nine-membered rings were observed on pressure increase up to 0.9 GPa (ref.

38, 1.0 GPa in ref. 39) and further pressure increase had little effect. They conclude that "VHDA represents the limit to densification by adapting the hydrogen-bonded network, without creating interpenetrating networks".[39]

Conclusions

The most surprising aspect of this study of isobaric annealing in high-density amorphous ice is a pronounced inflection in the *in situ* density *versus* pressure plot at ∼0.8 GPa (Fig. 2): below ∼0.8 GPa the slope is 0.21 g cm^{-3} GPa^{-1}, above ∼0.8 GPa the slope decreases to about half of the value. Parallel studies of recovered annealed samples by Raman spectroscopy and X-ray diffraction show that irreversible structural changes on isobaric annealing are most pronounced below ∼0.8 GPa, whereas above that pressure only minor structural changes occur. We conclude that mainly irreversible structural changes below ∼0.8 GPa lead to the pronounced increase in density, whereas above ∼0.8 GPa the density increase is dominated to a large extent by reversible elastic compression. This seems consistent with simulation studies by Martoňàk *et al.*[38] which indicate that annealing below 0.9 GPa involves substantial reconstruction of the topology of the hydrogen bonded network and changes in the ring statistics, whereas further pressure increase had little effect. Thus, we propose to call the rHDA states obtained on annealing at ∼ ≥ 0.8 GPa VHDA. We are confident that our *in situ* density values of rHDA are the most accurate ones reported in the literature and that these values should be used as reference in simulation studies of high-density amorphous ice and the effect of annealing on density. Finally we address the relationship between HDA and VHDA, that is whether VHDA "is a distinct phase, separated from HDA by a first-order transition, or whether it is simply very dense HDA".[9] In Fig. 2 the density of rHDA seems to increase continuously with increasing pressure, the abrupt change at ∼0.8 GPa indicating the pressure region where the irreversible densification has been nearly completed. This abrupt change of slope could indicate indeed formation of a distinct phase. A first-order phase transition requires a discontinuity in density which does not seem to occur. A second-order phase transition, which requires a change of slope in the volume (density) *versus* pressure plot, could be compatible with Fig. 2. However, within our experimental error it is difficult to discriminate between an abrupt and continuous and a discontinuous change of slope (see discussion in ref. 83).

Acknowledgements

References

1 O. Mishima, L. D. Calvert and E. Whalley, *Nature*, 1984, **310**, 393.
2 O. Mishima, L. D. Calvert and E. Whalley, *Nature*, 1985, **314**, 76.

396 | *Phys. Chem. Chem. Phys.*, 2006, **8**, 386–397

This journal is © the Owner Societies 2006

3 P. H. Poole, F. Sciortino, U. Essmann and H. E. Stanley, *Nature*, 1992, **360**, 324.

4 P. H. Poole, F. Sciortino, U. Essmann and H. E. Stanley, *Phys. Rev. E*, 1993, **48**, 3799.

5 H. E. Stanley, C. A. Angell, U. Essmann, M. Hemmati, P. H. Poole and F. Sciortino, *Physica A (Amsterdam)*, 1994, **206**, 1.

6 P. H. Poole, F. Sciortino, T. Grande, H. E. Stanley and C. A. Angell, *Phys. Rev. Lett.*, 1994, **73**, 1632.

7 P. G. Debenedetti, *Metastable Liquids*, Princeton University Press, Princeton, NJ, 1996.

8 O. Mishima and H. E. Stanley, *Nature*, 1998, **396**, 329.

9 P. G. Debenedetti, *J. Phys.: Condens. Matter*, 2003, **15**, R1669.

10 C. A. Angell, *Annu. Rev. Phys. Chem.*, 2004, **55**, 559.

11 E. Whalley, in *High-Density Amorphous Ice*, ed. G. W. Neilson and J. E. Enderby, Adam Hilger, Bristol, 1986.

12 L. Bosio, G. P. Johari and J. Teixeira, *Phys. Rev. Lett.*, 1986, **56**, 460.

13 A. Bizid, L. Bosio, A. Defrain and M. Oumezzine, *J. Chem. Phys.*, 1987, **87**, 2225.

14 M.-C. Bellissent-Funel, J. Teixeira and L. Bosio, *J. Chem. Phys.*, 1987, **87**, 2231.

15 H. Schober, M. Koza, A. Tölle, F. Fujara, C. A. Angell and R. Böhmer, *Physica B*, 1998, **241–243**, 897.

16 J. L. Finney, A. Hallbrucker, I. Kohl, A. K. Soper and D. T. Bowron, *Phys. Rev. Lett.*, 2002, **88**, 225503/1.

17 M. M. Koza, H. Schober, H. E. Fischer, T. Hansen and F. Fujara, *J. Phys.: Condens. Matter*, 2003, **15**, 321.

18 M. M. Koza, B. Geil, K. Winkel, C. Köhler, F. Czeschka, M. Scheuermann, H. Schober and T. Hansen, *Phys. Rev. Lett.*, 2005, **94**, 125506.

19 M. M. Koza, B. Geil, H. Schober and F. Natali, *Phys. Chem. Chem. Phys.*, 2005, **7**, 1423.

20 S. Klotz, T. Strässle, R. J. Nelmes, J. S. Loveday, G. Hamel, G. Rousse, B. Canny, J. C. Chervin and A. M. Saitta, *Phys. Rev. Lett.*, 2005, **94**, 025506.

21 J. S. Tse, D. D. Klug, M. Guthrie, C. A. Tulk, C. J. Benmore and J. Urquidi, *Phys. Rev. B*, 2005, **71**, 214107.

22 Y. P. Handa, O. Mishima and E. Whalley, *J. Chem. Phys.*, 1986, **84**, 2766.

23 M. A. Floriano, Y. P. Handa, D. D. Klug and E. Whalley, *J. Chem. Phys.*, 1989, **91**, 7187.

24 O. Mishima, *J. Chem. Phys.*, 1994, **100**, 5910.

25 O. Mishima, *J. Chem. Phys.*, 2004, **121**, 3161.

26 D. D. Klug, O. Mishima and E. Whalley, *J. Chem. Phys.*, 1987, **86**, 5323.

27 E. Whalley, *J. Less-Common Met.*, 1988, **140**, 361.

28 H. Kanno, K. Tomikawa and O. Mishima, *Chem. Phys. Lett.*, 1998, **293**, 412.

29 Y. Suzuki, Y. Takasaki, Y. Tominaga and O. Mishima, *Chem. Phys. Lett.*, 2000, **319**, 81.

30 O. Mishima and Y. Suzuki, *Nature*, 2002, **419**, 599.

31 O. V. Stal'gorova, E. L. Gromnitskaya, V. V. Brazhkin and A. G. Lyapin, *JETP Lett.*, 1999, **69**, 694.

32 E. L. Gromnitskaya, O. V. Stal'gorova, V. V. Brazhkin and A. G. Lyapin, *Phys. Rev. B*, 2001, **64**, 094205.

33 G. P. Johari and O. Andersson, *J. Chem. Phys.*, 2004, **120**, 6207.

34 O. Andersson and A. Inaba, *Phys. Chem. Chem. Phys.*, 2005, **7**, 1441.

35 O. Mishima, *Science*, 1991, **254**, 406.

36 N. Giovambattista, H. E. Stanley and F. Sciortino, *Phys. Rev. Lett.*, 2003, **91**, 115504.

37 B. Guillot and Y. Guissani, *J. Chem. Phys.*, 2003, **119**, 11740.

38 R. Martoňák, D. Donadio and M. Parrinello, *Phys. Rev. Lett.*, 2004, **92**, 225702.

39 R. Martoňák, D. Donadio and M. Parrinello, *J. Chem. Phys.*, 2005, **122**, 134501.

40 O. Mishima, *Nature*, 1996, **384**, 546.

41 E. Whalley, D. D. Klug and Y. P. Handa, *Nature*, 1989, **342**, 782.

42 J. S. Tse, *J. Chem. Phys.*, 1992, **96**, 5482.

43 J. S. Tse, D. D. Klug, C. A. Tulk, I. Swainson, E. C. Svensson, C.-K. Loong, V. Shpakov, V. R. Belosludov, R. V. Belosludov and Y. Kawazoe, *Nature*, 1999, **400**, 647.

44 T. Loerting, C. Salzmann, I. Kohl, E. Mayer and A. Hallbrucker, *Phys. Chem. Chem. Phys.*, 2001, **3**, 5355.

45 D. D. Klug, *Nature*, 2002, **420**, 749.

46 J. L. Finney, D. T. Bowron, A. K. Soper, T. Loerting, E. Mayer and A. Hallbrucker, *Phys. Rev. Lett.*, 2002, **89**, 205503.

47 S. Klotz, G. Hamel, J. S. Loveday, R. J. Nelmes, M. Guthrie and A. K. Soper, *Phys. Rev. Lett.*, 2002, **89**, 285502.

48 S. Klotz, T. Strässle, A. M. Saitta, G. Rousse, G. Hamel, R. J. Nelmes, J. S. Loveday and M. Guthrie, *J. Phys.: Condens. Matter*, 2005, **17**, S967.

49 A. M. Saitta, T. Strässle, G. Rousse, G. Hamel, S. Klotz, R. J. Nelmes and J. S. Loveday, *J. Chem. Phys.*, 2004, **121**, 8430.

50 N. Giovambattista, H. E. Stanley and F. Sciortino, *Phys. Rev. E*, 2005, **72**, 031510/1.

51 N. Giovambattista, H. E. Stanley and F. Sciortino, *Phys. Rev. Lett.*, 2005, **94**, 107803/1.

52 N. Giovambattista, P. G. Debenedetti, F. Sciortino and H. E. Stanley, *Phys. Rev. E*, 2005, **71**, 061505/1.

53 M. Guthrie, C. A. Tulk, C. J. Benmore and D. D. Klug, *Chem. Phys. Lett.*, 2004, **397**, 335.

54 J. K. Christie, M. Guthrie, C. A. Tulk, C. J. Benmore, D. D. Klug, S. N. Taraskin and S. R. Elliott, 2005.

55 I. Brovchenko, A. Geiger and A. Oleinikova, *J. Chem. Phys.*, 2003, **118**, 9473.

56 I. Brovchenko, A. Geiger and A. Oleinikova, *J. Chem. Phys.*, 2005, **123**, 044515.

57 C. Salzmann, E. Mayer and A. Hallbrucker, *Phys. Chem. Chem. Phys.*, 2004, **6**, 5156.

58 C. A. Tulk, C. J. Benmore, J. Urquidi, D. D. Klug, J. Neuefeind, B. Tomberli and P. A. Egelstaff, *Science*, 2002, **297**, 1320.

59 M. Guthrie, J. Urquidi, C. A. Tulk, C. J. Benmore, D. D. Klug and J. Neuefeind, *Phys. Rev. B*, 2003, **68**, 184110.

60 G. P. Johari and O. Andersson, *Phys. Rev. B*, 2004, **70**, 184108.

61 O. Andersson and G. P. Johari, *J. Chem. Phys.*, 2004, **121**, 3936.

62 I. Kohl, E. Mayer and A. Hallbrucker, *Phys. Chem. Chem. Phys.*, 2001, **3**, 602.

63 I. Kohl, *Amorphes festes Wasser hoher Dichte und sein Phasenübergang zu Eis XII*, PhD Thesis, University of Innsbruck, 2001.

64 C. G. Salzmann, T. Loerting, I. Kohl, E. Mayer and A. Hallbrucker, *J. Phys. Chem. B*, 2002, **106**, 5587.

65 D. L. Bish and S. A. Howard, *J. Appl. Crystallogr.*, 1988, **21**, 86.

66 V. F. Petrenko and R. W. Whitworth, *Physics of Ice*, Oxford University Press, 1999.

67 W. F. Kuhs, D. V. Bliss and J. L. Finney, *J. Phys. Colloq. C1*, 1987, **48**, 631.

68 B. Kamb, W. C. Hamilton, S. J. LaPlaca and A. Prakash, *J. Chem. Phys.*, 1971, **55**, 1934.

69 R. L. McFarlan, *J. Chem. Phys.*, 1936, **4**, 253.

70 C. Lobban, J. L. Finney and W. F. Kuhs, *J. Chem. Phys.*, 2000, **112**, 7169.

71 H. Engelhardt and B. Kamb, *J. Chem. Phys.*, 1981, **75**, 5887.

72 J. D. Londono, W. F. Kuhs and J. L. Finney, *J. Chem. Phys.*, 1993, **98**, 4878.

73 S. J. LaPlaca, W. C. Hamilton, B. Kamb and A. Prakash, *J. Chem. Phys.*, 1973, **58**, 567.

74 W. F. Kuhs, J. L. Finney, C. Vettier and D. V. Bliss, *J. Chem. Phys.*, 1984, **81**, 3612.

75 B. Kamb, *Science*, 1965, **150**, 205.

76 C. Lobban, J. L. Finney and W. F. Kuhs, *Nature*, 1998, **391**, 268.

77 S. Klotz, G. Hamel, J. S. Loveday, R. J. Nelmes and M. Guthrie, *Z. Kristallogr.*, 2003, **218**, 117.

78 J. M. Besson, P. Pruzan, S. Klotz, G. Hamel, B. Silvi, R. J. Nelmes, J. S. Loveday, R. M. Wilson and S. Hull, *Phys. Rev. B*, 1994, **49**, 12540.

79 C. A. Tulk, H. Kiefte, M. J. Clouter and R. E. Gagnon, *J. Phys. Chem. B*, 1997, **101**, 6154.

80 T. Strässle, S. Klotz, J. S. Loveday and M. Braden, *J. Phys.: Condens. Matter*, 2005, **17**, S3029.

81 F. D. Murnaghan, *Finite Deformation of an Elastic Solid*, Dover Press, New York, 1967.

82 C. A. Tulk, D. D. Klug, R. Branderhorst, P. Sharpe and J. A. Ripmeester, *J. Chem. Phys.*, 1998, **109**, 8478.

83 P. G. Debenedetti, *Nature*, 1998, **392**, 127.

This journal is © the Owner Societies 2006

Phys. Chem. Chem. Phys., 2006, **8**, 386–397 | 397